Nuclear Instruments and Methods in Physics Research A306 (1991) 112–122
North-Holland

Dynamics of skew beams and the projectional emittance *

Chun Fai Chan, William S. Cooper, Joe W. Kwan, and William F. Steele
Accelerator and Fusion Research Division, Lawrence Berkeley Laboratory, 1 Cyclotron Road, Berkeley, CA 94720, USA

Received 27 June 1990 and in revised form 3 January 1991

Study of the projectional emittance is an efficient way of probing the quality of a particle beam. In this work we deal with some computational aspects of the problem. We present the argument that in a beam optic code for the design or evaluation of the performance of electrostatic extractors/accelerators which produce such (round) beams, one must include in the calculation beamlets with skew angles. This is necessary if one wants to compare calculations with emittance measurements for a beam with transverse temperature. We have developed new steps and modified an existing code for such a purpose and produced calculated results of emittance plots that can be compared with experimental observations.

1. Introduction

An intense particle beam is usually formed by the extraction and acceleration of particles emanating from an emitter or source. In many applications, one prefers a beam with uniform intensity and low divergence. One way of studying the quality of the beam is to examine its transverse phase space intensity distribution in, e.g. x–x' (the projectional emittance [1]), using an emittance scanner [2–6]. The principal elements of the scanner consist of two slits placed perpendicular to the propagating direction of the beam. One slit allows a portion of the beam to pass to measure the x coordinate of that portion. Another slit, located somewhat further downstream, measures the angle with respect to the beam axis (the x' coordinate) and a detector behind the second slit measures the intensity. By moving the second slit transversely, different values of x' and intensity are recorded for the given x. Thus, by varying x and x', an emittance plot is produced. In this paper we concern ourselves with the computational aspect that arises from the consideration of the design of the extractor (accelerator) of a round beam using an axisymmetric electrostatic lens system, and how the computation is related to the emittance measurement method mentioned above. From this study we hope that we learn how to obtain a good quality beam for the desired application or for further acceleration. In general terms the procedure of our study is as follows: A beam optic code is used to trace the beam through the accelerator under study, and a phase space distribution in r–r' at a certain location is obtained. Then this is converted into a distribution in x–x' space that can be used to compare with a measured projectional emittance if desired.

For a beam with finite temperature, it becomes necessary to include particle motion in the azimuthal direction (the *skew* velocity component) in addition to motion in the radial and axial directions. The reason for this is explained in section 2. On the other hand, before the beam tracing starts, we have to have a scheme to represent a continuous 3-D velocity distribution (Maxwellian in our case) with a finite number of beamlets. One such method is presented in section 3. Because of the skew velocity component, we have to modify the usual 2-D axisymmetric beam tracing code [7] in order to correctly handle the particle motion. This is described in section 4. The mapping from r–r' space to x–x' space mentioned above is presented in sections 5 and 6. Finally, in section 7, some results of the calculations are compared with data from an H^- accelerator in our experiment.

It should be mentioned also that the beam dynamics presented is nonrelativistic because this work is concerned with the low energy acceleration of an ion beam (up to several hundred keV). We leave the generalization to relativistic motion (e.g., more appropriate to an electron beam), to a future study.

2. The necessity of skew beams

Suppose we have a particle beam emerging from a circle around the origin in the x–y plane of an emitter with its axis along the z direction as shown in fig. 1.

* This work was supported by USASDC MIPR W31RPP-63-A087 and the Director, Office of Energy Research, Office of Fusion Energy, Development and Technology Division, of the U.S. Department of Energy under Contract No. DE-AC03-76SF00098.

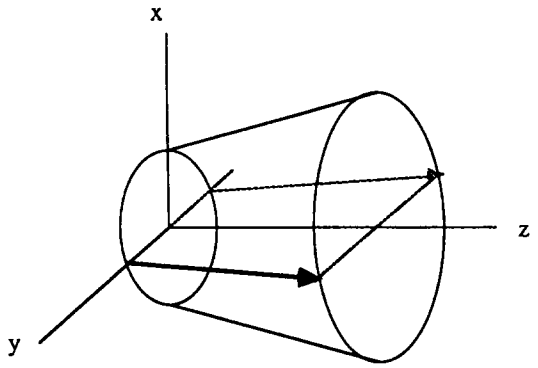

Fig. 1. Schematic drawing of a particle beam in which the beamlets have no skew velocity component.

Each point within the circle emits particles which shall be represented by *beamlets* in the scheme explained in the following sections. (The "emitter" of the particles does not need to be a flat disc, but we shall use it for now for simplicity). Next consider the coordinate system in fig. 2. A beamlet starting at point 0 has in general a velocity vector

$$v = v_r\hat{r} + v_\theta\hat{\theta} + v_z\hat{z}, \tag{1}$$

where $v_\theta = r\dot{\theta}$ is what we call the *skew velocity*. Now suppose that all the beamlets in fig. 1 have no such velocity component. All those starting at $x = 0$, for all y, have $x' = 0$ (recall that $x' = \mathrm{d}x/\mathrm{d}z$), whereas those starting at $x \neq 0$ have finite x'. Thus, in the x–x' phase plot, we should see a distribution like the one sketched in fig. 3. This is clearly different from what we observe in our measurement of projectional emittances, a typical shape of which is sketched in fig. 4. On the other hand, if those beamlets starting at $x = 0$ have skew velocity components and therefore have nonzero x', then they

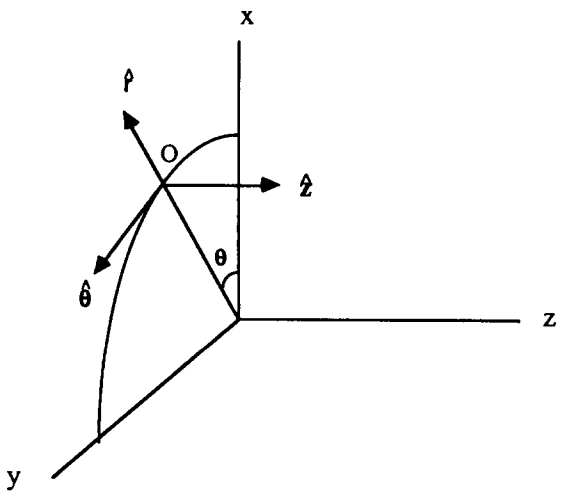

Fig. 2. Coordinate system.

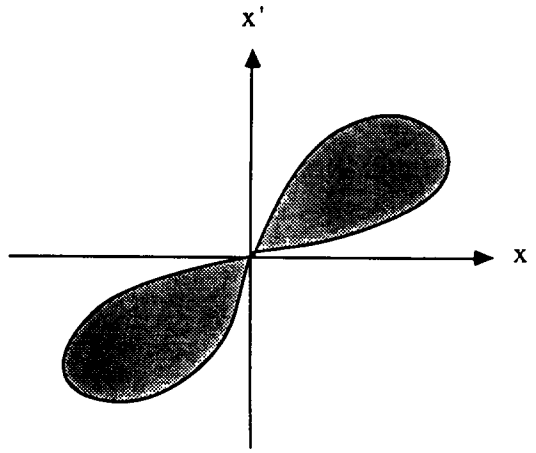

Fig. 3. Sketch of the shape of the projectional emittance produced by the beam shown in fig. 1.

can contribute to the width of the emittance plot on the x' axis. Thus, the discrepancy can be resolved by including in the analysis beamlets with skew angles, which carry the information about the transverse temperature of the beam.

Since any particle beam in nature has a temperature (or some kind of transverse energy spread), a correct, precise beam tracing code should take skew beamlets into account. There exist several codes that handle the optics of particle beams [7], but to our knowledge, this issue has not been addressed before.

3. Representing a 3-D drifting Maxwellian velocity distribution with a finite number of beamlets

In this section we shall work out a method for representing the starting condition for the computation

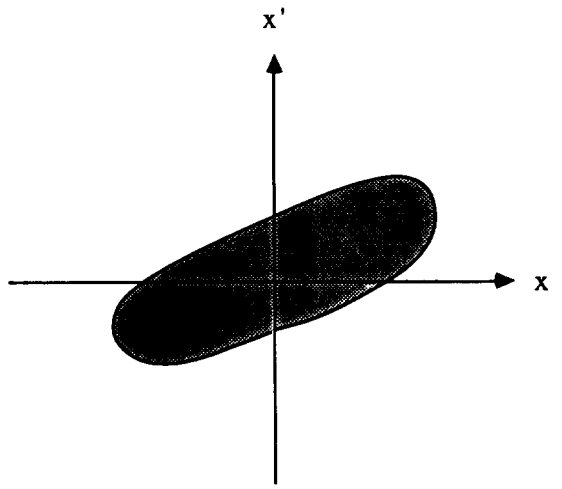

Fig. 4. Sketch of the shape of the projectional emittance observed in a typical experiment with a real particle beam.

of skew beam dynamics. Suppose that each point in the disc emitter in fig. 1 produces a certain current density carried by particles with a Maxwellian velocity distribution. How should we represent them with a finite number of beamlets?

Let the particles have a velocity distribution function f given by [8]

$$f = \exp\left[-\left(\frac{v_r}{u}\right)^2 - \left(\frac{v_\theta}{u}\right)^2 - \left(\frac{v_z - v_0}{u}\right)^2\right], \tag{2}$$

where

$$v_\theta = r\dot{\theta} = \text{the skew velocity}, \tag{3}$$

$$u = \left(\frac{2kT_i}{m}\right)^{1/2}, \tag{4}$$

$$kT_i = \text{the particle temperature}, \tag{5}$$

$$v_0 = \left(\frac{2E_0}{m}\right)^{1/2} = \text{the initial drift velocity}, \tag{6}$$

and we have ignored the normalization factor in f because it does not concern us in the following development. Define, for a beam moving in the $+z$ direction

$$\boldsymbol{J}_+ = \int_{-\infty}^{\infty} \mathrm{d}v_r \int_{-\infty}^{\infty} \mathrm{d}v_\theta \int_0^{\infty} \mathrm{d}v_z\, \boldsymbol{v} f, \tag{7}$$

$$n_+ = \int_{-\infty}^{\infty} \mathrm{d}v_r \int_{-\infty}^{\infty} \mathrm{d}v_\theta \int_0^{\infty} \mathrm{d}v_z\, f, \tag{8}$$

$$I_+ = \boldsymbol{J}_+ \cdot \mathrm{d}\boldsymbol{A}, \tag{9}$$

where $\mathrm{d}\boldsymbol{A} = |\mathrm{d}\boldsymbol{A}|\hat{z}$ is a surface element of the emitter.

Let us first outline the general scheme of beamlet representation and then illustrate it with an example. We divide $\boldsymbol{J}_+$ into $N \times N$ beamlets,

$$\boldsymbol{J}_{KL} = \int_{v_{r\,K}}^{v_{r\,K+1}} \mathrm{d}v_r \int_{v_{\theta\,L}}^{v_{\theta\,L+1}} \mathrm{d}v_\theta \int_0^{\infty} \mathrm{d}v_z\, \boldsymbol{v} f, \tag{10}$$

where

$$K, L = 1, \cdots, N,$$

and a similar equation holds for n_{KL}. The divisions are imposed in such a way that each beamlet carries the same current. We define

$$I_{KL} = \boldsymbol{J}_{KL} \cdot \mathrm{d}\boldsymbol{A}, \tag{11}$$

and we demand that the I_{KL}s equal each other for all K, L. This condition leads to simple equations for the $v_{r,K}$s and $v_{\theta,L}$s, which can be solved easily. The beamlets so obtained have the following properties:

$$\sum_{K,L} \boldsymbol{J}_{KL} = \boldsymbol{J}_+, \tag{12}$$

$$I_{KL} = \frac{1}{N^2} I_+, \quad \text{for the magnitude of the current carried by each beamlet, and} \tag{13}$$

$$\langle \boldsymbol{v}_{KL} \rangle = \frac{\boldsymbol{J}_{KL}}{n_{KL}}, \quad \text{for the beamlet directions.} \tag{14}$$

Next we show an example of 5×5 representation. For the first integral in eq. (10), we choose two parameters, α_1, α_2, whose values are to be determined. Therefore, we have five ranges of integration,

$$\int_{-\infty}^{-\alpha_1}, \quad \int_{-\alpha_1}^{-\alpha_2}, \quad \int_{-\alpha_2}^{\alpha_2}, \quad \int_{\alpha_2}^{\alpha_1} \quad \text{and} \quad \int_{\alpha_1}^{\infty}.$$

We have similar plans for the second integral in eq. (10) with the corresponding parameters β_1, β_2. Then we evaluate eq. (10) explicitly. The results are

$$\boldsymbol{J}_{KL} = \hat{r} c_1 g(\gamma) E_{\alpha K} F_{\beta L} + \hat{\theta} c_1 g(\gamma) F_{\alpha K} E_{\beta L} + \hat{z} c_1 h(\gamma) F_{\alpha K} F_{\beta L}, \tag{15}$$

$$n_{KL} = c_2 g(\gamma) F_{\alpha K} F_{\beta L}, \tag{16}$$

$$\frac{\langle \boldsymbol{v}_{KL} \rangle}{u} = \hat{r} c_3 \frac{E_{\alpha K}}{F_{\alpha K}} + \hat{\theta} c_3 \frac{E_{\beta L}}{F_{\beta L}} + \hat{z} c_3 \frac{1}{\sqrt{G}}, \tag{17}$$

where

$$c_1 = \frac{\pi}{8} u^4, \quad c_2 = \frac{\pi\sqrt{\pi}}{8} u^3, \quad \text{and} \quad c_3 = \frac{1}{\sqrt{\pi}},$$

$$\gamma = \frac{v_0}{u} = \left(\frac{E_0}{kT_i}\right)^{1/2}, \tag{18}$$

$$\mathrm{erf}(\gamma) = \frac{2}{\sqrt{\pi}} \int_0^{\gamma} \mathrm{d}t\, \mathrm{e}^{-t^2} = \text{the error function},$$

$$g(\gamma) = 1 + \mathrm{erf}(\gamma), \tag{19}$$

$$h(\gamma) = \mathrm{e}^{-\gamma^2} + \sqrt{\pi}\,\gamma g(\gamma), \tag{20}$$

$$\sqrt{G} = \frac{g(\gamma)}{h(\gamma)}, \tag{21}$$

$$E_{\alpha 1} = -\mathrm{e}^{-\alpha_1^2},$$

$$E_{\alpha 2} = -\mathrm{e}^{-\alpha_2^2} + \mathrm{e}^{-\alpha_1^2},$$

$$E_{\alpha 3} = 0,$$

$$E_{\alpha 4} = -\mathrm{e}^{-\alpha_1^2} + \mathrm{e}^{-\alpha_2^2},$$

$$E_{\alpha 5} = \mathrm{e}^{-\alpha_1^2},$$

$$F_{\alpha 1} = -\mathrm{erf}(\alpha_1) + 1, \quad F_{\alpha 2} = -\mathrm{erf}(\alpha_2) + \mathrm{erf}(\alpha_1),$$

$$F_{\alpha 3} = 2\,\mathrm{erf}(\alpha_2), \quad F_{\alpha 4} = \mathrm{erf}(\alpha_1) - \mathrm{erf}(\alpha_2),$$

$$F_{\alpha 5} = 1 - \mathrm{erf}(\alpha_1),$$

and the $E_{\beta L}$, $F_{\beta L}$ are same functions with α_1 and α_2 replaced by β_1 and β_2.

The condition eq. (11) requires that all the products $F_{\alpha K} F_{\beta L}$ equal each other. It is logically simple to require that all the $F_{\alpha K}$s equal each other, and the same for the $F_{\beta L}$s. This leads to identical conditions for the αs and βs. For the αs, we have two independent conditions,

$$1 - \mathrm{erf}(\alpha_1) = \mathrm{erf}(\alpha_1) - \mathrm{erf}(\alpha_2), \tag{22}$$

$$1 - \mathrm{erf}(\alpha_1) = 2\,\mathrm{erf}(\alpha_2). \tag{23}$$

This gives

$$\mathrm{erf}(\alpha_1) = \tfrac{3}{5}, \quad \mathrm{erf}(\alpha_2) = \tfrac{1}{5}. \tag{24}$$

Thus $\alpha_1 = 0.5951$, $\alpha_2 = 0.1792$, and $F_{\alpha K} = \frac{2}{5}$ for all K. We have the same results for β_1, β_2 and the $F_{\beta L}$s. From these we obtain the $\hat{r}$, $\hat{\theta}$ components of the velocity ratio, independent of the drift velocity v_0,

$$\left.\frac{\langle v_{KL}\rangle}{u}\right|_{\hat{r},\hat{\theta}} = -0.9898, -0.3761, 0.0000, 0.3761, 0.9898. \tag{25}$$

The $\hat{z}$ component of the velocity ratio in eq. (17) depends on the drift velocity v_0 through the quantity G. It can easily be evaluated once the values of kT_i and v_0 are given. For small and large values of v_0, we have the limits

$$\left.\frac{\langle v_{KL}\rangle}{u}\right|_{z} \begin{cases} \xrightarrow{v_0 \to 0} \dfrac{1}{\sqrt{\pi}} = \dfrac{1}{2}\dfrac{\langle v\rangle}{u}, \\ \quad \text{where } \langle v\rangle = \left(\dfrac{8kT_i}{\pi m}\right)^{1/2}, \end{cases} \tag{26}$$

$$\xrightarrow{v_0 \to \infty} \frac{v_0}{u} = \left(\frac{E_0}{kT_i}\right)^{1/2}. \tag{27}$$

For a representation with more than 5×5 beamlets, the situation is not a great deal more complicated. For example, for 11×11 representation, we have five αs with the conditions

$$\mathrm{erf}(\alpha_1) = \tfrac{9}{11}, \ \mathrm{erf}(\alpha_2) = \tfrac{7}{11}, \cdots, \mathrm{erf}(\alpha_5) = \tfrac{1}{11}.$$

We have tested a 45×45 representation (together with the mapping formula described in section 5); the results are shown in appendix B.

We should remark that, for the purpose of "beam launching", the method described in this section is sufficient, but not necessary. There are other methods [9], each with some advantages and disadvantages.

To conclude, with the magnitudes of beamlet currents given by eq. (13) and directions given by eq. (14), we are ready to start the beam tracing provided that we have the correct beam dynamics to take into account the skew motion.

4. Skew beam dynamics

With the initial condition of the beam specified by the method described above, suppose now it enters a region of external electrostatic force. Let the Lagrangian of a particle of the beam be [10]

$$L = \tfrac{1}{2}m(\dot{r}^2 + r^2\dot{\theta}^2 + \dot{z}^2) - qV(r, z), \tag{28}$$

where we have assumed that V has no θ dependence for an axisymmetric situation. Then the equations of motions are

$$mr^2\dot{\theta} = J = \text{const.}, \tag{29}$$

$$m\ddot{r} = \frac{J^2}{mr^3} - q\frac{\partial V}{\partial r}, \tag{30}$$

$$m\ddot{z} = -q\frac{\partial V}{\partial z}. \tag{31}$$

In eq. (29), J is the angular momentum of the particle due to skew motion. Eqs. (30) and (31), together with the Poisson equation [8]

$$\nabla^2 V = -\frac{1}{\epsilon_0}n, \tag{32}$$

form the basis of our new beam tracing code. It is still a 2-D code, involving only r and z coordinates. The method of obtaining the space charge density n from the beamlet currents is described in detail in ref. [7]. The fields $-\partial V/\partial r$, $-\partial V/\partial z$ are treated either as constants or linear functions of coordinates within mesh units imposed on (r, z). Solving eq. (30) exactly within a unit would involve elliptic integral, which is quite messy. In practice, we use an approximation by replacing the r in the centrifugal force term in eq. (30) with r_0, the starting value in the unit, or with $(r_1 + r_2 + r_3)/3$ when we use a triangular mesh.

5. Mapping from r–r' phase space to x–x' phase space

After we run the beam tracing code for a certain problem, with ingredients outlined in previous sections, we obtain a plot of the distribution of points in r–r' space for a chosen location in z. Now we want to convert this distribution into a corresponding distribution in x–x' space to construct a projectional emittance.

First, let us consider the total current in the phase space. Suppose ρ_4 is the current intensity distribution [1] in transverse phase space. Then the total current I is the integral of this distribution,

$$I = \int \mathrm{d}x\, \mathrm{d}y\, \mathrm{d}x'\, \mathrm{d}y'\, \rho_4(x, y, x', y'), \tag{33}$$

$$= \int r\, \mathrm{d}r\, \mathrm{d}\theta\, \mathrm{d}r'\, \mathrm{d}\alpha'\, \rho_4(r, \theta, r', \alpha'), \tag{34}$$

where (see fig. 2)

$$x' = \frac{\mathrm{d}x}{\mathrm{d}z} = \frac{v_x}{v_z}, \quad r' = \frac{\mathrm{d}r}{\mathrm{d}z} = \frac{v_r}{v_z}, \quad \alpha' = r\frac{\mathrm{d}\theta}{\mathrm{d}z} = \frac{v_\theta}{v_z},$$

and

$$r^2 = x^2 + y^2, \quad r'^2 + \alpha'^2 = x'^2 + y'^2.$$

The relations between the two coordinate systems [1] are

$$x' = r' \cos\theta - \alpha' \sin\theta, \qquad y' = r' \sin\theta + \alpha' \cos\theta. \tag{35}$$

The inverse relations are

$$r' = x'\frac{x}{r} + y'\frac{y}{r}, \qquad \alpha' = -x'\frac{y}{r} + y'\frac{x}{r}, \tag{36}$$

with

$$\cos\theta = \frac{x}{r}, \quad \sin\theta = \frac{y}{r} = \sqrt{1 - \frac{x^2}{r^2}}.$$

Now, if we have a point in r–r' space with coordinates r_1, r_1', skew velocity α_1' and current

$$I_1 = 2\pi r_{10}\, \Delta r_{10} J_{10}, \tag{37}$$

where r_{10} = the initial radius of the ring of current when the beamlet starts, Δr_{10} = the width of the ring, and J_{10} = the initial current density carried by the beamlet, then

$$\rho_4 = \frac{I_1}{2\pi r}\delta(r - r_1)\delta(r' - r_1')\delta(\alpha - \alpha_1'). \tag{38}$$

Put this ρ_4 into eq. (34), after some calculus, (see appendix A), and since [1] $\rho_2 = \mathrm{d}^2 I/\mathrm{d}x\,\mathrm{d}x'$, we have

$$\rho_2(x, x') = \int \mathrm{d}y\,\mathrm{d}y'\rho_4 = \frac{I_1}{\pi r_1}\frac{1}{\sqrt{1 - \frac{x^2}{r_1^2}}} \times \delta\left[x' - \left(\frac{r_1'}{r_1}x - \alpha_1'\sqrt{1 - \frac{x^2}{r_1^2}}\right)\right]. \tag{39}$$

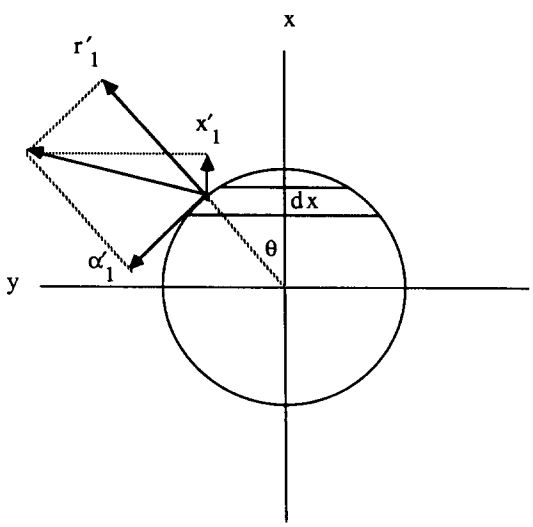

Fig. 5. Geometric meanings of the factors in eq. (39).

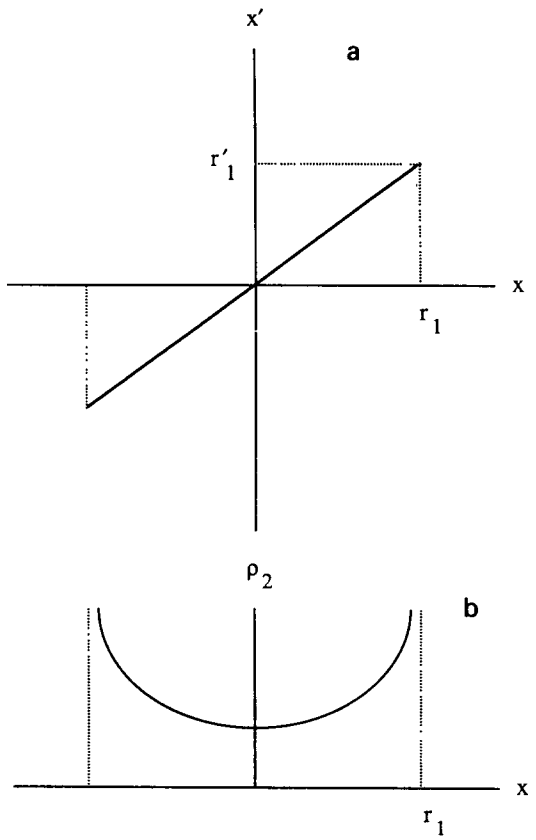

Fig. 6. (a) A point in (r, r') is mapped into a line in (x, x') by eq. (40). (b) The intensity factor in eq. (39).

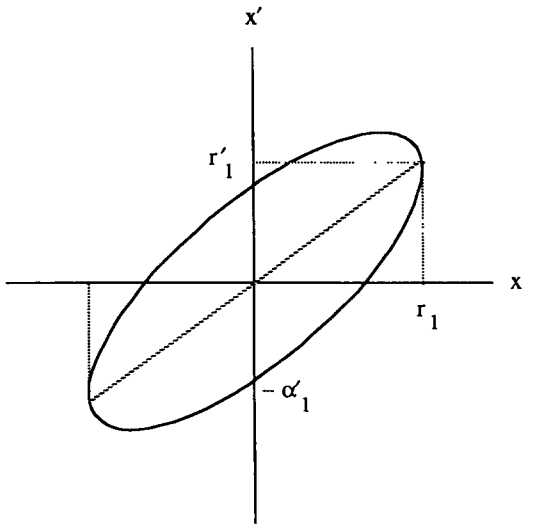

Fig. 7. A point in (r, r') is mapped into a half-ellipse in (x, x') by eq. (41).

There is a simple geometric interpretation for every factor in eq. (39). One can easily verify the following: the factors preceding the δ function give the portion of the current ring passed through the slit with width dx. The length of the arc is just $dx/\sin\theta$ (see fig. 5). And the argument in the δ function is just the condition that the angle x' is due to the combined motions in the radial and skew directions.

If there is no skew velocity, $\alpha_1' = 0$, and the argument of the δ function gives

$$x' = \frac{r_1'}{r_1} x. \tag{40}$$

That is, a point in r–r' space is mapped into a straight line passing through the origin in x–x' space as shown in fig. 6a, with intensity distribution sketched in fig. 6b. The sum of the contributions from these phase points would give a plot that looks like the one sketched in fig. 3.

If there is skew velocity, $\alpha_1' \neq 0$, and

$$x' = \frac{r_1'}{r_1} x - \alpha_1' \sqrt{1 - \frac{x^2}{r_1^2}}\,. \tag{41}$$

A point in r–r' space is mapped into a half-ellipse (see fig. 7). If $\alpha_1' > 0$, we get the half that is below the line eq. (40). (It should be noted that this line is not the major axis of the tilted ellipse.) Specifically, from eq. (41), we get

$$\left(a^2 + \frac{b^2}{r_1^2}\right) x^2 - 2axx' + x'^2 = b^2, \tag{42}$$

where $a = r_1'/r_1$, and $b = \alpha_1'$.

Next we consider the value of α_1'. After the beam optics calculation, we obtain the final values r_1, r_1' for the phase point at location z. The value of $\langle v_\theta \rangle_1$ is obtained by using eq. (29) and the initial values r_{10}, $\langle v_\theta \rangle_{10}$,

$$\langle v_\theta \rangle_1 = \frac{r_{10}}{r_1} \langle v_\theta \rangle_{10}. \tag{43}$$

Recall that $\langle v_\theta \rangle_{10}$ is determined by the beam initial temperature kT_i, therefore eq. (43) takes care of the accounting of beam heating due to radial compression or cooling due to expansion. Thus,

$$b = \alpha_1' = \left(\frac{r_{10}}{r_1}\right)\left(\frac{\langle v_\theta \rangle}{u}\right)_{10} \sqrt{\frac{kT_i}{E_z}}\,, \tag{44}$$

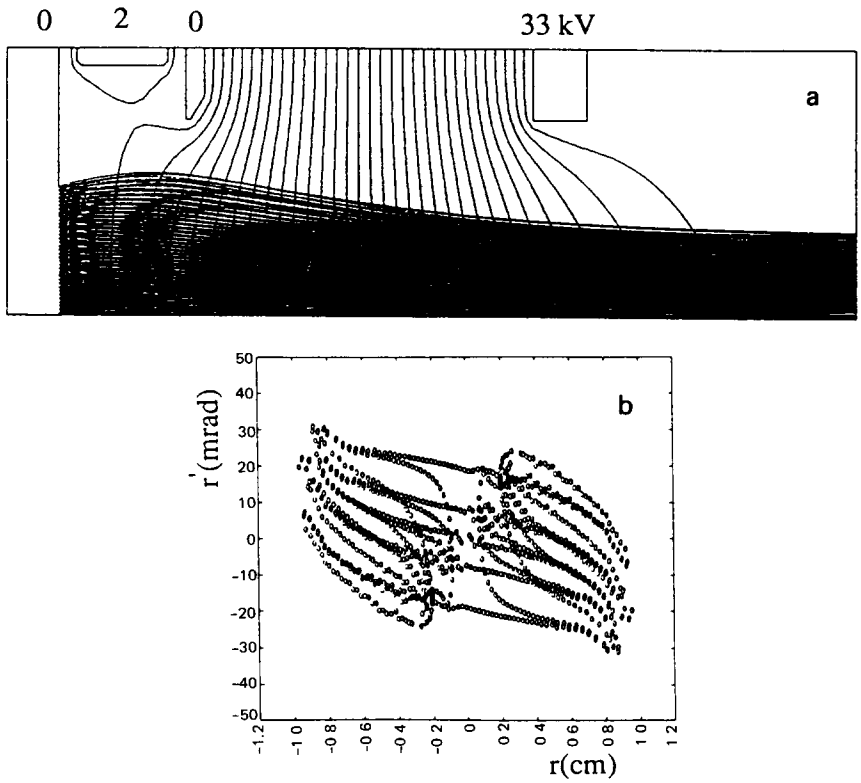

Fig. 8. Trajectory and exit r–r' phase plots of a H^- ion beam from an axisymmetric electrostatic accelerator. We use $35\times5\times5$ beamlets in r–r'–α' space. (Ion beam optics with skew beams. $r = 1.456$ cm, $E = 33$ kV, $p = 13$ mT, $I = 31$ mA. Assumptions: $kT_i = 4$ eV, uniform j at the emitter). (a) All beams. (b) Phase space in r–r'.

where $(\langle v_\theta \rangle / u)_{10}$ is the input value from eq. (14), (see also the example in eq. (17)), and E_z is the beam energy at the phase plot location. Notice that b is just the intercept of the half-ellipse with the x' axis.

6. Practical implementation of the mapping

In order to do the mapping in practice, we have to impose a grid in the x–x' plane. Suppose we integrate eq. (39) from x_i to x_{i+1}, then

$$\left.\frac{\Delta^2 I}{\Delta x\, \Delta x'}\right|_{ij} = \frac{I_1}{\pi r_1}\left[\sin^{-1}\left(\frac{x_{i+1}}{r_1}\right) - \sin^{-1}\left(\frac{x_i}{r_1}\right)\right]. \quad (45)$$

We deposit this amount of current, say, at the lower left corner of the grid cell under consideration: (x_i, x'_j), where x'_j is given by eq. (41), in which x takes the value of x_i. In order to calculate the contribution of one point (r_1, r'_1) to ρ_2 on the whole grid, it is necessary to calculate the intersections of the half ellipse of eq. (42) with the grid lines.

7. Application of the method and comparison of the results with data

We have studied a test case for the mapping formula eq. (39), as well as for the beamlet representation described in section 3, with a "flat-Maxwellian" distribution which has a known analytic solution. The result is quite satisfactory and it is presented in appendix B.

Next we apply the method to calculate the performance of an accelerator of H^- ions for magnetic fusion energy or other applications [11]. In the example presented below, we choose to use a $35 \times 5 \times 5$ beamlet representation in r–r'–α' space due to computer time limitations. The initial velocity components are given by eq. (25) in section 3. In fig. 8 we show the trajectory plot of all the beamlets and the r–r' phase plot at the beam exit location. The H^- ions start their paths from the "emitter" at the left hand side. An emitter in this case is the assumed plasma boundary, with the requirement that the electric field there is low ($\lesssim 1000$ V/cm). The source plasma, located to the left of this boundary,

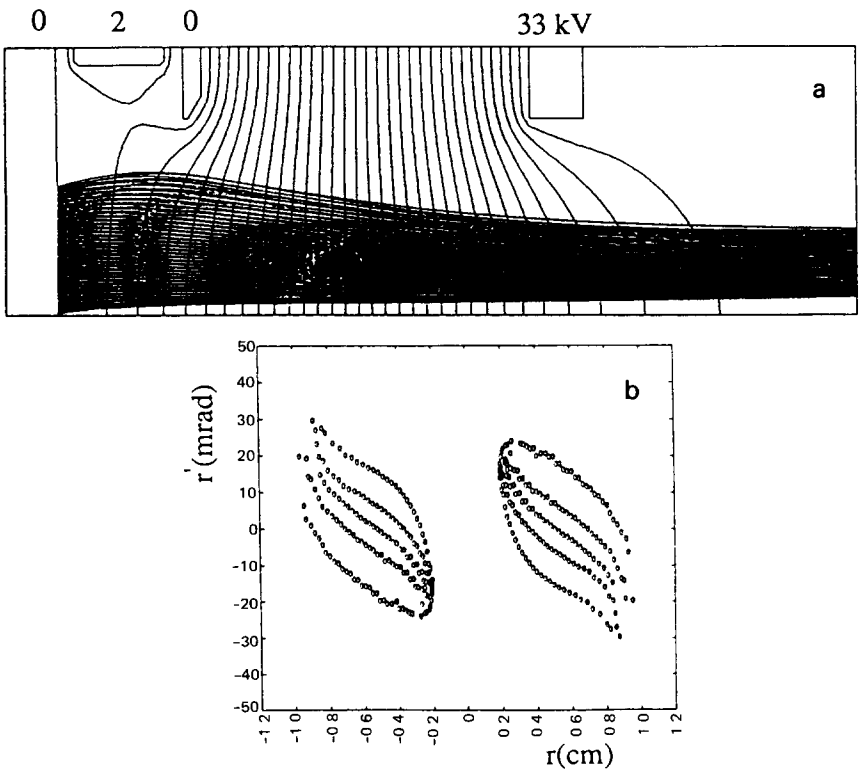

Fig. 9. A subset of beamlets in fig. 8, corresponding to $35 \times 5 \times 2$ in r–r'–α' space, with $\langle v_\theta \rangle / u = \pm 0.9898$. (Ion beam optics with skew beams. $r = 1.456$ cm, $E = 33$ kV, $p = 13$ mT, $I = 31$ mA. Assumptions: $kT_i = 4$ eV, uniform j at the emitter). (a) One set of skew beams. (b) Phase space in r–r'.

actually also contains positive ions and electrons. Their effect on this calculation is believed to be not significant and therefore is neglected. Our goal here is not to do a detailed comparison of the calculation with data, but rather to demonstrate the utility of the method. Therefore, a simplified physical picture mentioned above is adopted and we content ourselves with the following preliminary comparison.

In fig. 9, we show the trajectory plot and the corresponding exit phase plot for one set of beamlets with $\langle v_\theta \rangle / u$ equal to ± 0.9898, (see eq. (25)). This shows the effect of the centrifugal force term, which makes the beamlets "leave" the axis.

Accompanying the r–r' phase plot of fig. 8 is a table (not shown) that contains, for each point, the values of r_1, r_1', α_1', and I_1 as described in section 5. We use the mapping formula eq. (45) to generate another table that contains the intensity distribution in x–x' phase space. Finally, a computer program developed by one of us (W.F.S.) is used to produce a percentage contour plot, shown in fig. 10. The measured intensity distribution, processed by the same contour plotting program, is shown in fig. 11.

As one can see, there is quite a change in appearance in going from the r–r' phase plot in fig. 8 to the x–x' projectional emittance shown in fig. 10. The result is reasonably close to the measured projectional emittance shown in fig. 11. We believe that even better agreement could be achieved by using more refined physical input for the calculation; we leave that for future investigations.

There are two technical points that should be addressed. First, the emittance data shown in fig. 11 is not centered at the origin because there is a magnetic field at the upstream part of the accelerator to sweep out the

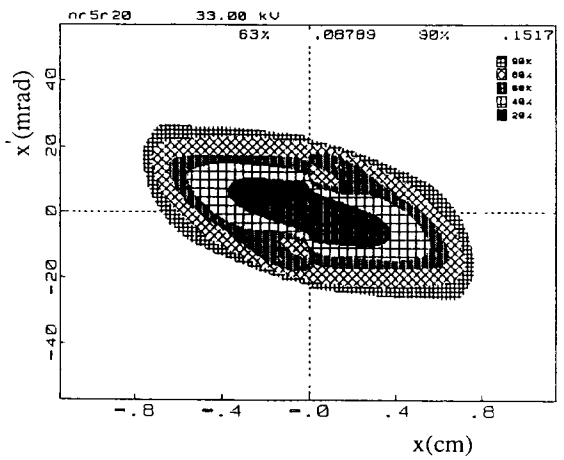

Fig. 10. Projectional emittance plot converted from the r–r' phase plot in fig. 8 with the averaging procedure described in appendix C.

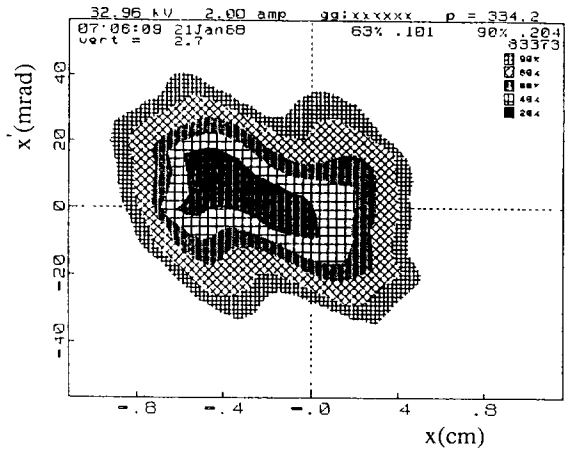

Fig. 11. Projectional emittance plot from experimental measurement.

unwanted electrons, which are extracted together with the H^- ions. This deflects the ion beam somewhat and causes the shift of the center of the plot. (We ignore this effect in the calculation, too.)

The second point is that, in order to produce fig. 10, we have used a method of averaging in x–x' phase space. As we mentioned at the beginning of this section, we used only a 5×5 beamlet representation in r'–α' space for the problem in fig. 8; this was due to computer time limitations in tracing a large number of beamlets over some distance. This is far less than the 45×45 representation we used in the simple test problem in appendix B. The 5×5 representation, however, produces too much fluctuation in intensity ρ_2 over the x–x' grid and does not give a smooth-looking contour plot. We use the method of averaging to smooth out the initial result. This is explained in appendix C. We should emphasize that the use of this procedure is not strictly necessary but it is economical to do so. In our experience with several other cases of applications of the work described in this paper, this method works rather well.

8. Discussions and conclusions

The main results of this paper are the 3-D beamlet representation scheme, the inclusion of the centrifugal force term in the 2-D beamlet dynamics and the mapping formula. We have shown that by including skew beamlets in the beam optic calculation, we are able to obtain a projectional emittance that can be compared with experimental observation. Furthermore, for reasonable assumptions of the initial beam properties, the calculated projectional emittances agree reasonably well with experimentally measured ones. Without the inclusion of skew beamlets, the comparison is poor.

The centrifugal force term is inversely proportional to r^3; thus it effects strongly only on those beamlets near the axis. The resulting change in overall space charge distribution is relatively small because those beamlets also carry smaller amounts of current (recall that each beamlet actually represents a ring of current in our axisymmetric system.) It is for this reason that ion optics codes that do not include skew beamlets can be used successfully in many cases for design purposes, even though they predict incorrect projectional emittances.

Next let us discuss the question of maximal change in angle in going from r–r' space to x–x' space due to skew motion. Applying $\partial x'/\partial x = 0$ to eq. (41), we obtain the maximal values

$$x_m = \frac{r_1}{\sqrt{1+\left(\frac{\alpha_1'}{r_1'}\right)^2}}, \tag{46}$$

$$x_m' = r_1'\sqrt{1+\left(\frac{\alpha_1'}{r_1'}\right)^2}. \tag{47}$$

Thus, the angle is increased by the square root factor. From the expression for α_1' given by eq. (44), we see that the increment is contributed to by various factors. In the case we studied in section 7, the increase is only a few percent. In cases where one has large beam compression ratio and high temperature, the effect would be larger.

Acknowledgements

We would like to thank Wulf B. Kunkel for helpful comments. One of us (C.F.C.) thanks Phrank Chan for his assistance in preparing the manuscript.

Appendix A

Derivation of the mapping formula

In section 5 we have

$$\rho_2(x,x') = \int \mathrm{d}y\,\mathrm{d}y' \frac{I_1}{2\pi r}\delta(r-r_1)\delta(r'-r_1')\delta(\alpha'-\alpha_1'). \tag{A.1}$$

Recall that

$$\delta(f(y)) = \sum_i \frac{1}{\left|\frac{\partial f}{\partial y}\right|_{y=y_{0i}}}\delta(y-y_{0i}), \tag{A.2}$$

where $f(y_{0i}) = 0$, therefore

$$\delta(r-r_1) = \left|\frac{r_1}{y_{1+}}\right|\delta(y-y_{1+}) + \left|\frac{r_1}{y_{1-}}\right|\delta(y-y_{1-}),$$

where $y_{1\pm} = \pm\sqrt{r_1^2 - x^2}$.

We have a similar formula for $\delta(r'-r_1')$. Notice, however, that the choice of

$$y_{1\pm}' = \pm\sqrt{r_1'^2 - x'^2 - \alpha_1'^2}$$

is not independent of the choice of $y_{1\pm}$, in view of eq. (35) and the assumption that we have an axisymmetric beam. Therefore, we have only two terms (instead of four terms),

$$\begin{aligned}\delta(r-r_1)\delta(r'-r_1') &= \left|\frac{r_1}{y_{1+}}\right|\left|\frac{r_1'}{y_{1+}'}\right|\delta(y-y_{1+})\delta(y'-y_{1+}') \\ &\quad + \left|\frac{r_1}{y_{1-}}\right|\left|\frac{r_1'}{y_{1-}'}\right|\delta(y-y_{1-})\delta(y'-y_{1-}').\end{aligned} \tag{A.3}$$

Putting eq. (A.3) into eq. (A.1), we obtain

$$\rho_2(x,x') = \frac{I_1}{2\pi r_1}\frac{r_1 r_1'}{y_1 y_1'}\left[\delta\left(-x'\frac{y_1}{r_1} + y_1'\frac{x}{r_1} - \alpha_1'\right) + \delta\left(x'\frac{y_1}{r_1} - y_1'\frac{x}{r_1} - \alpha_1'\right)\right], \tag{A.4}$$

where $y_1 = |y_{1\pm}|$ and $y_1' = |y_{1\pm}'|$.

Now, if $\alpha_1' = 0$, the two δ functions combine to form 2δ because of the relation $\delta(-x) = \delta(x)$. If $\alpha_1' \neq 0$, then because α_1' is symmetrically distributed around the beam axis, we can always find another beamlet with $\alpha' = -\alpha_1'$, so that eq. (A.4) can be simplified, without double counting,

$$\rho_2(x,x') = \frac{I_1}{2\pi r_1}\frac{r_1 r_1'}{y_1 y_1'}2\delta\left(-x'\frac{y_1}{r_1} + y_1'\frac{x}{r_1} - \alpha_1'\right). \tag{A.5}$$

From the relation $x^2 + y^2 = r^2$, we obtain $xx' + y_1 y_1' = r_1 r_1'$. This relation, together with eqs. (35) and (36), enables us to use eq. (A.2) to transform the δ function in eq. (A.5) into the following from:

$$\delta\left(-x'\frac{y_1}{r_1} + y_1'\frac{x}{r_1} - \alpha_1'\right) = \frac{y_1'}{r_1'}\delta\left[x' - \left(\frac{r_1'}{r_1}x - \alpha_1'\sqrt{1-\frac{x^2}{r_1^2}}\right)\right]. \tag{A.6}$$

Thus, we obtain eq. (39).

Appendix B

Test of the mapping formula with a flat-Maxwellian distribution

A flat-Maxwellian distribution [8] is defined as

$$\rho_4 = \rho_0(x,y)\exp\left[-(\dot{x}^2+\dot{y}^2)/u^2\right], \tag{B.1}$$

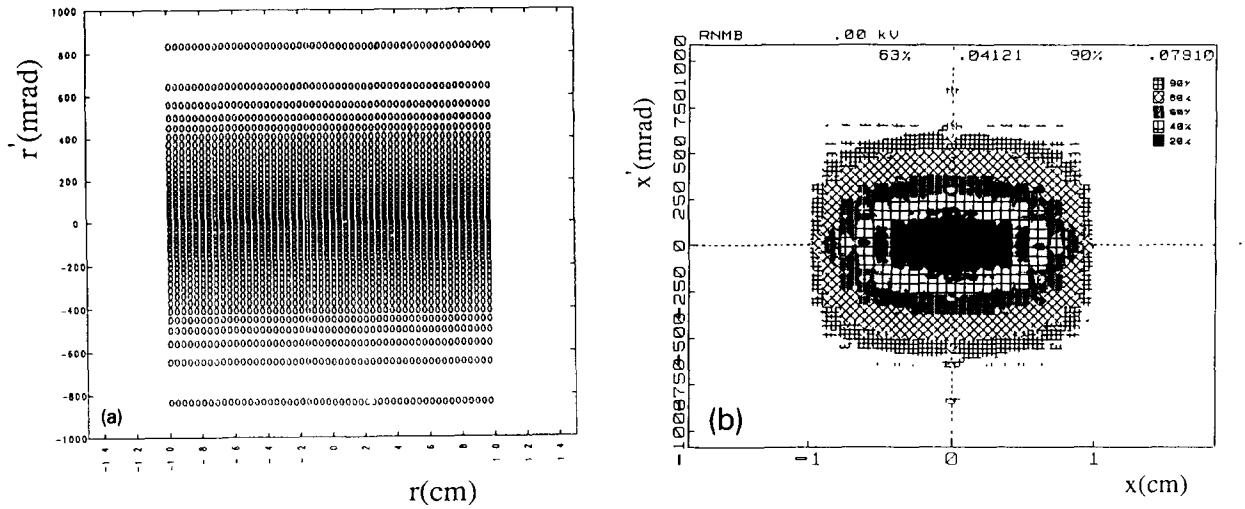

Fig. 12. (a) $r-r'$ phase plot of a flat-Maxwellian distribution. (b) Projectional emittance plot converted from the plot in (a). Starting from the center of the plot, it shows the areas for 20, 40, 60, 80 and 90% of the total current.

where $\rho_0(x, y) = \text{const.}$ for $r \le r_0$, $\dot{x} = \mathrm{d}x/\mathrm{d}t$, etc., and u is given by eq. (4). Then after the integration over y and $\dot{y}$, we have

$$\rho_2 = a\sqrt{r_0^2 - x^2}\exp\left[-x'^2/b^2\right], \tag{B.2}$$

where $b^2 = 2kT_i/\beta^2 mc^2$, $\beta = \dot{z}/c$, $a = 2\sqrt{\pi}\, b\rho_0$, and $x' = \mathrm{d}x/\mathrm{d}z$ as before.

For the test we consider a "pill-box" problem in which an ion beam, with initial conditions: radius = 1 cm, $kT_i = 1.5$ eV and $E_0 = 6.0$ eV, propagates only a short distance in z. In this way, we obtain an initial phase plot without actually having to go through the beam dynamic part of our program. In order to gain sufficient fineness and accuracy we choose to use a relatively large number of beamlets for this test problem. Namely, in $r-r'-\alpha'$ we use $25 \times 45 \times 45$ beamlets.

In fig. 12a we show the $r-r'$ phase plot. Each point in this plot represents, in addition to the r, r' values shown, an intensity given by eq. (37) and one of the 45 skew velocity components. Feeding all these quantities into eq. (45) and choosing a 100×100 grid in $x-x'$, we obtain a matrix of ρ_2 values. Then with the help of a percentage contour plotting code we generate fig. 12b, the projectional emittance computed from discrete beamlets. One can see that the contours in this plot are quite similar to those contours of $\rho_2 = \text{const.}$ in ref. [8].

From the matrix of ρ_2 values, we have also computed $\langle x^2 \rangle$ and $\langle x'^2 \rangle$. The magnitudes are very close to those obtained from the analytic formula [8]. We remark also that figs. 12a and 12b are the typical plots of the initial phase of an ion beam entering an accelerator.

Appendix C

The method of averaging in $x-x'$ space

As we explained at the end of section 7, an auxiliary averaging procedure is used to smooth out the result from the mapping calculation in the case when we use an economical but undesirably small number of beamlets in the representation of a continuous velocity distribution. We used an averaging procedure in which the intensity value in eq. (45) at each point in the $x-x'$ grid, whenever it is nonzero, is replaced by the average of its

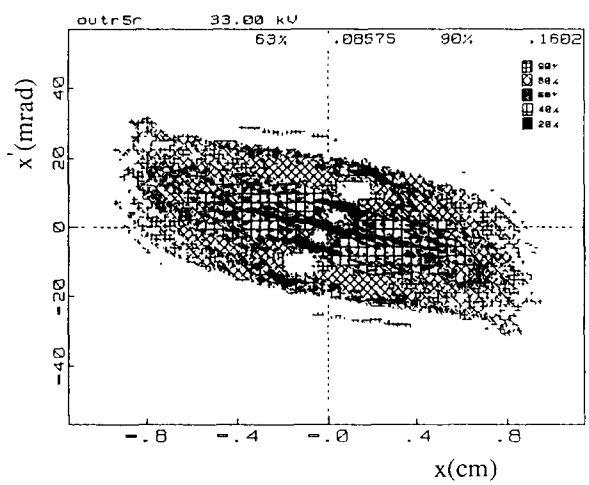

Fig. 13. Projectional emittance plot converted from the $r-r'$ phase plot in fig. 8 without the averaging procedure.

own intensity plus those of the surrounding eight points. The "nonzero" condition is due to the fact that we want to apply this procedure only to the interior points of the emittance. This averaging process can be repeated a number of times as explained below.

In fig. 13, we show the "raw" result of the contour plot from the mapping calculation for the problem described in section 7. Notice that there are five dark streaks (corresponding to high intensities) in the x' direction. This is a consequence of the five beamlet representation in x' space. The gap widths between these streaks are $\lesssim 10$ mrad. The width of the grid cells in x' we used in this plot is 1 mrad (50 mrad/50 cells). If we define N_c to be the number of cells per gap, then

$$N_c = \frac{\text{gap width}}{\text{cell width}} \approx 10.$$

Then, in analog to a diffusion problem [12], we assert that in order for any information to disperse from one streak halfway to the next streak, in either direction, it has to take $(N_c/2)^2$ steps. Therefore, we choose the number of times to repeat the averaging process to be

$$N_{\text{avg}} = \left(\frac{N_c}{2}\right)^2 \approx 25.$$

In practice, the result is not sensitive to the exact value of N_{avg}. From fig. 13 we produce fig. 10 by using $N_{\text{avg}} = 20$. For each average, we use

$$\begin{aligned}\rho_{2,\text{new}}(i, j) &= \tfrac{1}{9}\big[\rho_2(i-1, j) + \rho_2(i, j) + \rho_2(i+1, j) \\ &\quad + \rho_2(i-1, j+1) + \rho_2(i, j+1) \\ &\quad + \rho_2(i+1, j+1) + \rho_2(i-1, j-1) \\ &\quad + \rho_2(i, j-1) + \rho_2(i+1, j-1)\big],\end{aligned}$$

provided $\rho_2(i, j) \neq 0$. Otherwise, we skip this process. We have also tried to do the average only in the x' (i.e., j) direction, but the results are not much different for the cases we studied.

This method of averaging is used only to smooth out the intensity fluctuation. It is a cheap way to "fill in with more beamlets" between the gaps. Obviously, we should not overdo it, or it will wash out the detail features of the emittance plot. On the other hand, if we are willing to use more beamlets, we can get smooth results without using this process, as we showed in the test case in appendix B.

References

[1] See, for example, Claude Lejeune and Jean Aubert, Emittance and Brightness: Definitions and Measurements, in Adv. Electron. Electron Phys., suppl. 13a, ed. A. Septier, part A (Academic Press, 1980) p. 159.
[2] A. van Steenbergen, Nucl. Instr. and Meth. 51 (1967) 245.
[3] L.L. Ames, Nucl. Instr. and Meth. 151 (1978) 363.
[4] J.H. Billen, Rev. Sci. Instr. 46 (1976) 33.
[5] J.H. Billen, Rev. Sci. Instr. 46 (1976) 1295.
[6] P.W. Allison, J.D. Sherman and D.B. Holtkamp, IEEE Trans. Nucl. Sci. NS-30 (4) (1983) 2204.
[7] We use the axisymmetric version of the code originally developed for a sheet beam by W.S. Cooper, K. Halbach and S.B. Magyary, Proc. 2nd Symp. on Ion Sources and Formation of Ion Beams, Berkeley, LBL-3399, 1974. See also K. Halbach, Mathematical Models and Algorithms for the Computer Program WOLF, LBL-4444 (1975) and the following article plus the references therein: P. Spädtke, Computer Modeling, in: The Physics and Technology of Ion Sources, ed I.G. Brown (Wiley, 1989) p. 107.
[8] J D. Lawson, The Physics of Charged Particle Beams (Clarendon, Oxford, 1977) p. 220.
[9] See, for example, Charles K Birdsall and A. Bruce Langdon, Plasma Physics via Computer Simulation (McGraw-Hill, 1985) p. 387.
[10] See, for example, H. Goldstein, Classical Mechanics, 2nd ed. (Addison-Wesley, MA, 1980).
[11] J.W. Kwan et al., Rev. Sci. Instr. 61 (1980) 369.
[12] F. Reif, Fundamentals of Statistical and Thermal Physics (McGraw-Hill, 1965) p. 17.